# Macroscopic and Microscopic Spray Characteristics of Diesel and Karanja Biodiesel Blends

**Conference Paper** *in* SAE Technical Papers · April 2016

DOI: 10.4271/2016-01-0869



**2 authors:**


Jai gopal Gupta
Indian Institute of Technology Kanpur



Avinash Kumar Agarwal
Indian Institute of Technology Kanpur

SAE INTERNATIONAL®

# Macroscopic and Microscopic Spray Characteristics of Diesel and Karanja Biodiesel Blends

2016-01-0869

Published 04/05/2016

**Jai Gopal Gupta and Avinash Kumar Agarwal**
Indian Institute of Technology Kanpur

**CITATION:** Gupta, J. and Agarwal, A., "Macroscopic and Microscopic Spray Characteristics of Diesel and Karanja Biodiesel Blends," SAE Technical Paper 2016-01-0869, 2016, doi:10.4271/2016-01-0869.



## Abstract

Fuel injection pressure (FIP) is one of the most important factors affecting diesel engine performance and particulate emissions. Higher FIP improves the fuel atomization, which results in lower soot formation due to superior fuel-air mixing. The objective of this spray study was to investigate macroscopic and microscopic spray parameters in FIP range of 500-1500 bar, using a solenoid injector for biodiesel blends (KB20 and KB40) and baseline mineral diesel. For these test fuels, effect of ambient pressure on macroscopic spray characteristics such as spray penetration, spray area and cone angle were investigated in a constant volume spray chamber (CVSC). Microscopic spray characteristics such as velocity distribution of droplets and spray droplet size distribution were measured in the CVSC at atmospheric pressure using Phase Doppler Interferometry (PDI). At higher fuel injection pressure (1500 bar) and 40 bar ambient pressure, biodiesel blends spray evolution was slower than baseline mineral diesel, suggesting its stronger atomization with smaller droplet size distribution and consequently the droplet momentum. The spray cone angle of mineral diesel was wider than biodiesel blends. Droplet size distribution represented by Sauter mean diameter ($D_{32}$) and arithmetic mean diameter ($D_{10}$) increased with increasing biodiesel concentration in the test fuel. Overall, these results are useful for explaining and comparing the biodiesel fuelled engine behavior.

## Introduction

Direct injection compression ignition (DICI) engine's emissions and performance characteristics are greatly influenced by the spray characteristics, which affect fuel-air mixing and resulting combustion. In order to improve fuel-air mixing, it is important to understand the fuel atomization and spray formation processes. It is well known that fuel injection pressure, drag force, physical properties of the fuel and ambient pressure govern fuel atomization and spray tip penetration. Among these factors, drag on fuel droplets, which is governed by the relative magnitude of the kinetic energy of individual droplets and the aerodynamic resistance of the surrounding gas are very important.

As the spray droplet velocity distribution and the ambient air density increase, aerodynamic and viscous effects become more important and the spray breakup process becomes more complex. Senator *et al.* [1] characterized the diesel like calibration fluid (ISO 4113), biodiesel of different origin and their blends such as (type A) RME, (type B) Rapeseed/ Soybean mixture (60/ 40%) and (type C) Rapeseed/ Used fried oils (UFO) mixtures (75/ 25%) for spray investigations. Results of spray tip penetration measurements were reported for (a) 1.2 MPa and (b) 5 MPa nitrogen back pressures with 120 MPa fuel injection pressure (FIP). They concluded weak interaction of droplets with the surrounding gas at 1.2 MPa for all test fuels. However, at 5 MPa, back pressure slowed the development of sprays for all test fuels. The ISO 4113 spray penetration results showed significantly lower values than biofuels, which is indicative of its stronger atomization with reduced droplet diameters and consequently the momentum [1].

Lee and Park [2] numerically investigated the effect of fuel injection pressure on the macroscopic spray behavior and atomization characteristics of high-pressure spray in a common rail type diesel injection system and compared it with the experimental results using particle motion analysis system and phase Doppler particle analyzer (PDPA). They reported that downstream of the spray, due to the large relative velocity between spray and ambient gas, outer droplets of the main spray disintegrated faster into the smaller droplets prior to the inner droplets [2]. Lacoste et al. [3] studied the effect of in-cylinder pressure, axial positions and fuel injection pressure on atomization characteristics of dense diesel spray. It was reported that higher FIP and in-cylinder pressures improve spray atomization, and an increase in mean droplet velocity and mean diameter was observed, when axial distance from the nozzle was increased [3].

Spray characteristics are predominantly affected by fuel properties such as surface tension, density and viscosity. Deeper understanding of relationship between spray characteristics and fuel's physical properties is essential for adopting new alternative fuels on a large scale worldwide. The differences in physical properties of mineral diesel and biodiesel are expected to significantly alter the inner nozzle flows and spray structure, thus affecting the performance and emission characteristics of the engine as well. Wang and Huang [4] reported that biodiesel gave deeper spray penetration and larger droplet sizes compared to mineral diesel, primarily due to its higher viscosity and surface tension. The effect of different physical properties on spray characteristics using different blends of biodiesel was investigated in their study.

Park *et al.* [5] performed spray visualization and PDPA experiments and reported that biodiesel yielded longer spray penetration due to its higher surface tension. Biodiesel hardly atomized compared to mineral diesel. Analyzing the relationship between fuel properties and engine performance, Kegl *et al.* [6] concluded that higher density, viscosity and lower vapor content of biodiesel under high pressure injection systems led to advancement fuel injection timing, which in-turn led to premature increase in in-cylinder pressure, temperature and rate of heat release compared to mineral diesel. They also reported that higher oxygen content of biodiesel resulted in lower smoke and CO emission with only slightly higher HC emissions.

Som *et al.* [7] characterized the inner nozzle flow dynamics of mineral diesel and biodiesel by simulation using mixture-based cavitation model. They reported that lower levels of cavitation and turbulence for biodiesel than mineral diesel were observed because of biodiesel's lower vapor pressure. Biodiesel showed poor atomization characteristics compared to mineral diesel. Spray penetration and SMD were marginally higher for biodiesel, while dispersion and cone angle were lower. The computed liquid lengths of mineral diesel and biodiesel were compared with the experimental data from Sandia National Laboratories. They observed higher liquid lengths for biodiesel due to its higher boiling temperature and heat of vaporization [7]. Though the simulations captured this trend well, the liquid lengths remained under-predicted, which was attributed to uncertainty about the properties of biodiesel used in the experiments. They also concluded from this study that the differences in the injection and spray behavior of the two fuels may require changes in the piston bowl design or in the injection and/or ambient conditions in order to use biodiesel in an existing diesel engine [7].

Lee *et al*. [8] studied the spray characteristics and common rail direct injection (CRDI) engine performance using biodiesel blends derived from unpolished rice bran oil biodiesel (BD20a and BD40a) and soybean oil biodiesel (BD20b and BD40b). Spray tip penetration, mean droplet size, velocity distributions, and injection profiles were measured using the spray visualization and PDPA system. They concluded that performance of diesel engine using biodiesels can be improved by optimizing the FIP and its timing [8]. It was also concluded that despite different physical properties of test fuels, very little differences were observed in the spray tip penetration in biodiesel blends. Higher surface tension and viscosity of biodiesel reduced Weber number and injection velocity respectively and led to inferior atomization and increasing droplet size compared to diesel. Use of biodiesel required high FIP to overcome friction between the fuel and nozzle wall because of biodiesel's higher viscosity. Higher friction leads to lower injection rate for biodiesel blended fuels [8].

Li *et al.* [9] performed experiments for microscopic spray characteristics of diesel, RME and Gas-to-Liquid (GTL) fuels in atmospheric conditions at different fuel injection pressures (80MPa to 150 MPa) and measuring positions varied from 20 mm to 70 mm downstream of nozzle using PDPA technique. Data rate was observed to be quite low in regions near the nozzle and at high FIP. Sauter Mean Diameter (SMD) of all fuel droplets decreased with increasing FIP. However, diesel spray showed a smaller SMD when injection pressure was increased to 120 MPa. The injection pressure had little effect on the radial velocity of droplets. SMD decreased with increasing axial distance downstream of nozzle for given fuels at FIP of 120 MPa, while it was relatively unaffected at 80 MPa FIP [9]. It was reported that the maximum droplet velocity increased with increasing FIP [9]. Regarding the difference in velocity development of the test fuels, diesel droplets arrival velocity was slightly higher than two other test fuels at 80 MPa. This was attributed to their relatively lower viscosity, even though pressure difference between FIP and the ambient pressure was the main factor, which determined the exit momentum. When the FIP increased from 80 MPa to 120 MPa, the arrival velocities of the three test fuels were almost similar [9].

The objective of this spray study is to investigate the effect of FIP in pressure range of 500-1500 bar and ambient pressure in spray chamber. For this, a solenoid injector was employed, which was also used in the experimental test engine (Tata; Safari DICOR 2.2 L). Fuel injection was characterized for macroscopic and microscopic spray parameters for biodiesel blends (KB20 and KB40) and mineral diesel was used as a baseline fuel. Effect of ambient pressure was investigated in a constant volume spray chamber (CVSC) for macroscopic spray characteristics such as spray penetration, spray area and spray cone angle for all test fuels. Microscopic spray characteristics such as spray droplet velocity distribution and spray droplet size distribution were measured in the CVSC at atmospheric pressure. Optical diagnostic techniques were used for macroscopic and microscopic spray characterization, which are non-intrusive but can often be complex to implement and expensive.

## Experimental Setup and Procedure

In order to analyze the influence of biodiesel on the spray atomization characteristics spray visualization, droplet size and velocity distribution were determined experimentally using varying fuel injection parameters on a CRDI fuel injector.

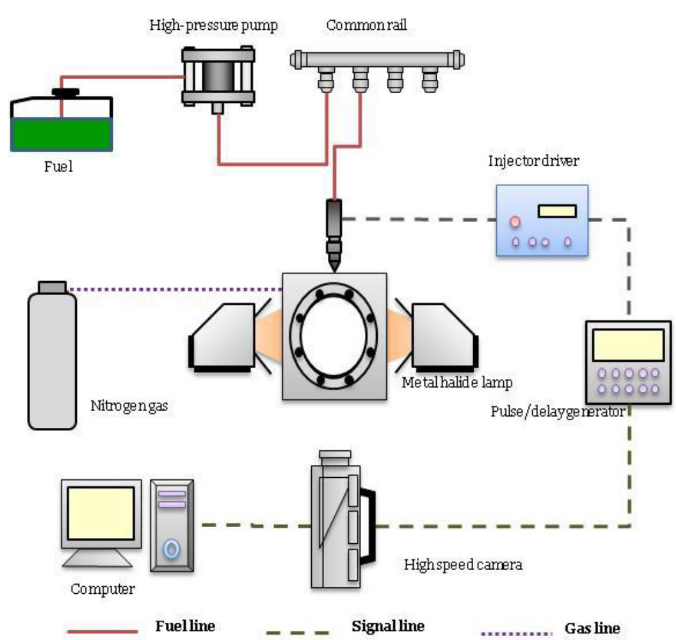


Figure 1. Schematic of the experimental setup for spray visualization

To analyze the macroscopic characteristics of test fuel spray, spray visualization system was used (Figure 1). A high-pressure, constant volume spray chamber (CVSC) with optical windows, which could be pressurize up to 60 bar was used for spray visualization. CVSC's ambient pressure was controlled in the range spraying from atmospheric to 40 bar using a nitrogen gas cylinder. Spray images were captured using high-speed camera (Photron; FASTCAM APX) after every 0.1 ms (10,000 fps) from the start of injection in the CVSC. Flicker-free white light source (NaBa Green model) was used for illuminating the fuel spray. The shutter of the high-speed camera was synchronized with the injector signal in order to capture spray images at a particular time after the start of needle lift in the injector. An injector driver which was a common rail solenoid injector peak and hold driver (ZB; 5100) and a digital delay and pulse generator (Berkeley Nucleonics; 575) was used for synchronization of the solenoid injector and the camera. Three images were taken and averaged at the same elapsed time to minimize the experimental errors. The spray images captured were stored in a computer using an image grabber. The test injector used in these experiments was a solenoid type common-rail injector (Delphi; Solenoid CRDI injector) with six holes having an injection angle of 156˚.

Spray velocity and droplet size distributions were determined by modular Phase Doppler interferometry (PDI) system (Artium; PDI-300 MD). PDI is a robust and non-intrusive technique for measuring droplet size and velocities in sprays [10] 11]. Measurement principle is based on light scattering interferometry, which utilizes the wavelength of light as the measurement scale. The parameters affecting the measurement are the laser light wavelength and focal lengths of the lenses in the transmitters and receiver [12]. PDI involves creating an interference pattern in the region where laser beams converge and spherical droplets are sprayed through the intersection point. This results in a region of alternate dark and bright fringes. The region where the beams intersect is called "Probe Volume' or "Sample Volume'. The light scattered, while passing through the probe volume, is received by the receiver, which converts the photonic signals to voltage signals and sends them to computer for further analysis. PDI measures the droplet size distribution, all three components of velocity, volume flux and droplet number density.

Figure 2 shows the schematic of the experimental setup for PDI system. The PDI instrument includes computer controlled diode-pumped solid-state (DPSS) lasers, frequency shifting modules, optical receiver with compact photo detectors, pre-amplifiers, ASA signal processing system, and an advanced Automated Instrument Management System (AIMS) software package. PDI transmitter contains green, blue and yellow lasers. The blue solid state laser emits radiations at 491 nm, green laser emits radiations at 532 nm and yellow laser emits radiations at 561 nm [12]. Transmitters also contain appropriate optics and Braggs cells, which shift the frequency and split each laser beam into two equal intensity beams. AIMS software performs full complex Fourier analysis for obtaining results of droplet size and velocity distribution. Optical receiver is synchronized with the fuel injector. Technical specifications and configuration parameters for PDI are given in Table 1 and 2 respectively.

A six holes solenoid injector, with only one open hole (one plume) and remaining five blocked holes, was used for the experiment. Injected fuel quantity was maintained constant at 12 mg per injection for all test conditions by varying the injection duration, using an Injector driver (NI Drivven; 780718-01) system.

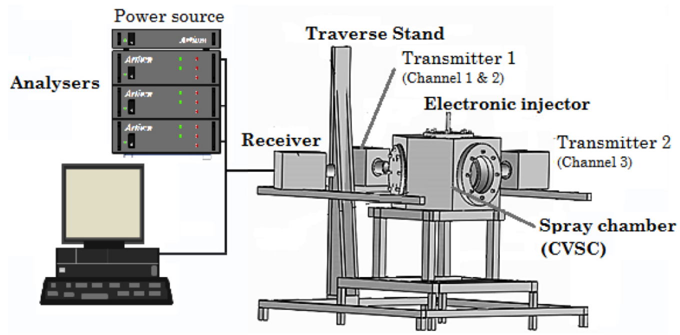


Figure 2. Schematic of the Phase Doppler Interferometry (PDI) system.

Table 1. Technical specifications of the modular PDI system [12]

| | |
|---|---|
| Droplet size measurement range | 0.5-2000 μm or larger |
| Accuracy | ± 0.5 μm |
| Resolution | ± 0.5 μm |
| Velocity Measurement Range | -100 to 300 m/s |
| Velocity Accuracy | ± 1% |
| Volume Flux Accuracy | ± 15% |
| Receiver Focal Length | 350, 500, 750, 1000 mm |
| Transmitter Focal Length | 350, 500, 750, 1000 mm |

Table 2. Configuration parameters for 3D PDI

| **Parameters** | **Channel 1 & Channel 2** | **Channel 3** | **Receiver** |
|---|---|---|---|
| Laser (Power), mW | 500 | 500 | - |
| Wavelength, nm | 532 (green), 491 (blue) | 561 (yellow) | - |
| Laser beam diameter, mm | 2.33, 2.33 | 2.33 | - |
| Beam separation, mm | 59.6, 60 | 60.49 | - |
| Beam expander factor | 1.0, 1.0 | 1.0 | - |
| Frequency shift, MHz | 40 | 45 | 40 |
| Lens Focal length, mm | 500 | 500 | 350 |
| Fringe spacing (δ), μm | 4.5, 4.1 | 4.6 | - |
| Photo detector voltage, V | 450 | 500 | - |
| Slit aperture, μm | - | - | 25 |
| Collection angle, ° | - | - | 30 |
| Processor auto-setup enabled | Yes | Yes | - |
| Index of refraction | - | - | 1.46 |
| Measurement diameter range, μm | 0-75 | - | - |
| Measurement velocity range, m/s | -30 to 100 | - | - |

The investigations on the test fuels were conducted 40 mm downstream from the nozzle hole, at varying injection pressures and ambient pressure in the CVSC. Experimental test matrix for spray characterization is given in table 3.

Table 3. Test matrix for spray characterization

| | |
|---|---|
| Test fuels | Diesel, KB20, KB40 |
| Injector make/ type | Delphi/ Solenoid CRDI injector |
| Number of the nozzle holes | 6 holes |
| Injection angle | 156˚ |
| Injection quantity (mg) | 12 |
| Injection pressure (bar) | 500, 750, 1000, 1250, 1500 |
| Ambient pressure (bar) (Visualization) | Atmospheric pressure, 20, 40 |
| Ambient pressure (bar) (PDI) | Atmospheric pressure |

## Results and Discussion

Table 4 shows viscosity, density and lower heating value (LHV) of test fuels of this study, namely mineral diesel, 20% blend of Karanja biodiesel (KB20), and 40% blend of Karanja biodiesel (KB40). Viscosity and density of fuels increased with increasing biodiesel concentration in the test fuel. Calorific value of the test fuels decreased with increasing biodiesel concentration.

Table 4. Important physical properties of test fuels

| **Test Fuel** | **Viscosity @ 40°C (cSt)** | **Density (g/cm$^3$)** | **LHV (MJ/kg)** |
|---|---|---|---|
| Diesel | 2.71 | 0.822 | 43.06 |
| KB20 | 3.31 | 0.835 | 42.52 |
| KB40 | 3.51 | 0.848 | 41.98 |
| KB100 | 5.79 | 0.887 | 40.36 |

Fuel injection pressure is one of the most important factors affecting the performance of a diesel engine and particulate emissions. Higher fuel injection pressure improves the fuel/air mixing and fuel vaporization, which results in the lower soot formation in the spray flames due to improved combustion characteristics [13].

### *Macroscopic Spray Characteristics*

The macroscopic parameters of fuel spray such as spray tip penetration, spray area and spray cone angle were obtained directly from the images captured by the spray visualization. In this study, spray tip penetration is defined as the maximum axial distance of the injected spray from the injection nozzle tip. The spray cone angle is defined as the largest angle formed by two straight lines from the nozzle tip to the boundary of the spray. The spray area defined as the area covered by fuel spray plume boundary.

Figure 3 shows the effect of variation in ambient pressure on spray tip penetration at 500, 750, 1000, 1250 and 1500 bar fuel injection pressure for mineral diesel, KB20 and KB40. In the spray visualization experiments, CVSC pressure was varied as 1, 20 and 40 bar using nitrogen.

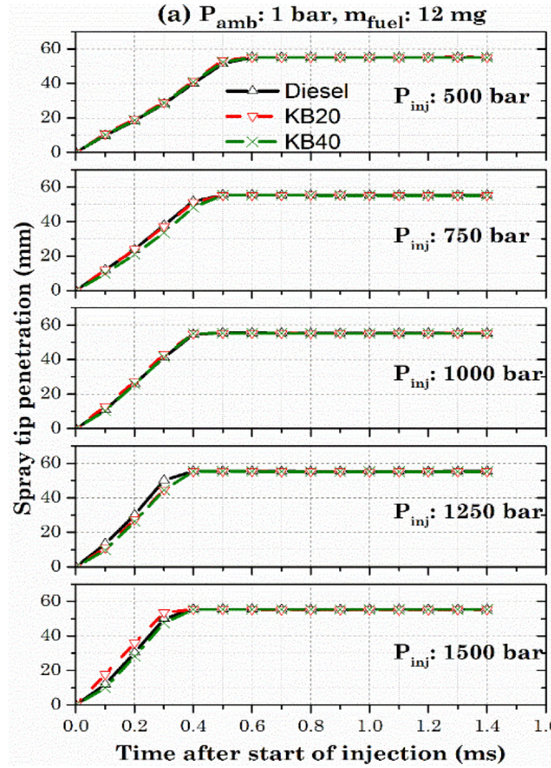


a.

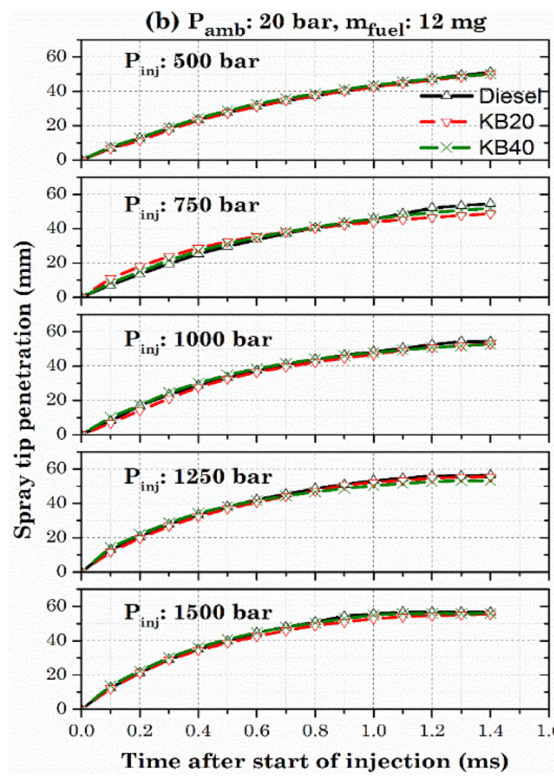


b.

Figure 3. Comparison of spray tip penetration for diesel, KB20 and KB40 at (a) 1 bar, (b) 20 bar and (c) 40 bar ambient pressure of spray chamber.

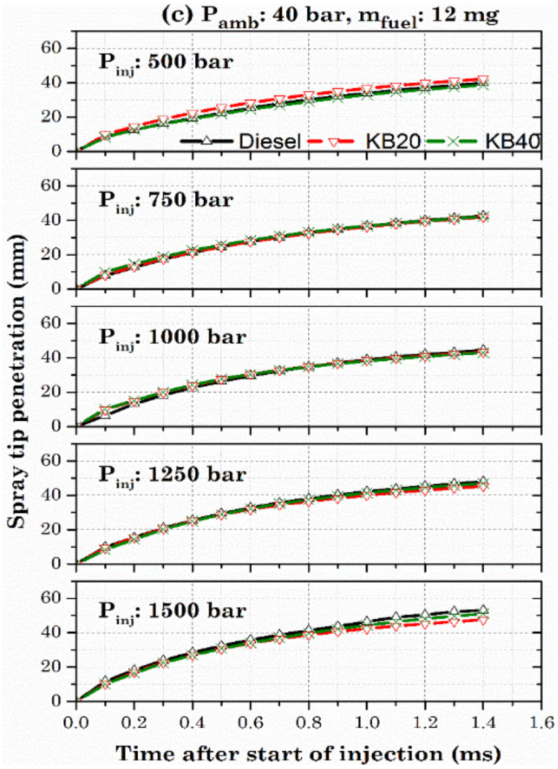


c.

Figure 3. (cont.) Comparison of spray tip penetration for diesel, KB20 and KB40 at (a) 1 bar, (b) 20 bar and (c) 40 bar ambient pressure of spray chamber.

The comparison of spray tip penetration according to biodiesel blending ratios showed quite similar relationship between mineral diesel and Karanja biodiesel blends, while variations in spray tip penetration due to variation in CVSC pressure and injection pressure showed significantly larger differences for the three test fuels. Figure 3a shows that at 1 bar ambient pressure in the CVSC, behavior of the curves is typical of the spray tip penetrations with an initial straight trend, meaning a weak interaction of the droplets of test fuels with the surrounding gas. After the start of injection, the curves tend towards saturation (55 mm) within 0.6 ms at 1 bar ambient pressure in CVSC. While spray penetration of 50 and 40 mm were attained later than 1.4 ms at 20 and 40 bar ambient pressure respectively in CVSC at 500 bar fuel injection pressure. The slope of curves reduced significantly with increasing ambient pressures (20 and 40 bar). Spray tip penetration remarkably reduced with increase in spray chamber pressure because of increased flow resistance between spray and ambient gas. This shows a strong breaking/ scattering of spray droplets due the ambient gas resistance in the CVSC. The fuels penetrate with difficulty in high-density gas and the curves tend to slowly toward saturate.

Almost similar variations in spray tip penetration results of biodiesel blends with time after start of injection from the nozzle were observed, due to slightly higher density and viscosity of Karanja biodiesel blends (Table 4). Higher viscosity of biodiesel increased friction between biodiesel and nozzle surface, which led to slower spray evolution initially. However, due to higher density, the momentum of biodiesel spray droplet is higher than mineral diesel, which makes the spray tip penetration of biodiesel blends longer than diesel in the later period of injection [14]. Therefore comparatively lower difference was observed in the spray penetration lengths of diesel and biodiesel blends at all test conditions.

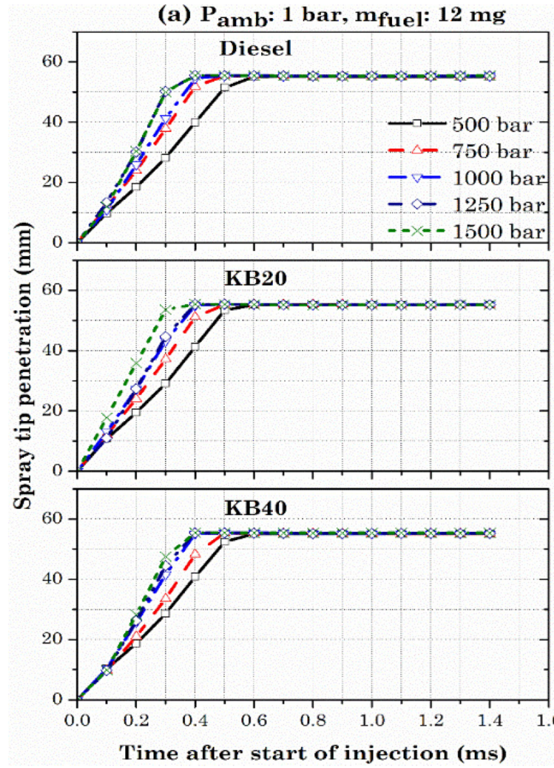


a.

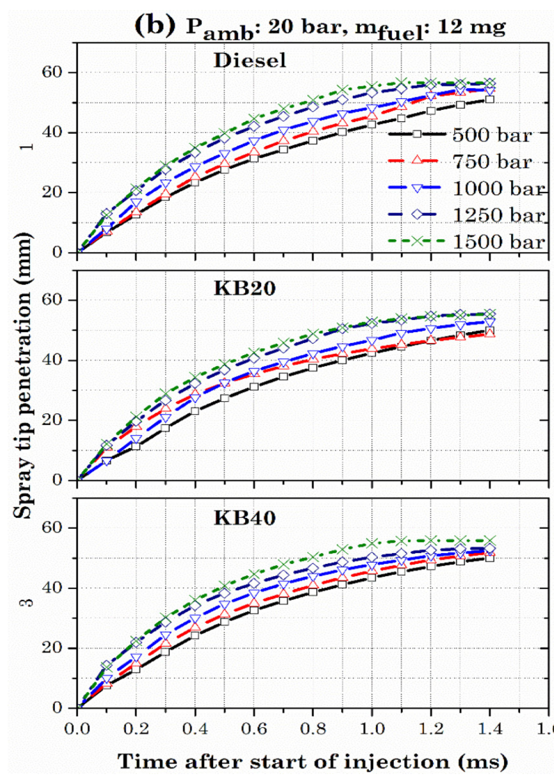


b.

Figure 4. Comparison of spray tip penetration at different fuel injection pressure for diesel, KB20 and KB40 at (a) 1 bar, (b) 20 bar and (c) 40 bar ambient pressure of spray chamber.

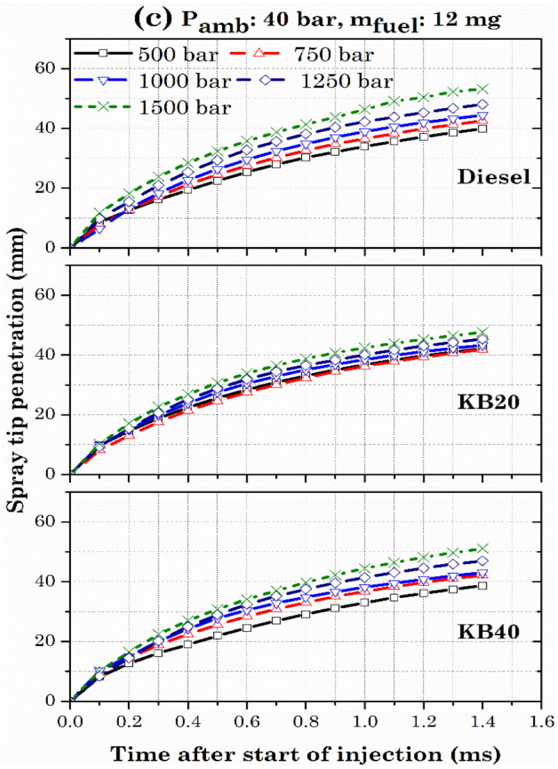


c.

Figure 4. (cont.) Comparison of spray tip penetration at different fuel injection pressure for diesel, KB20 and KB40 at (a) 1 bar, (b) 20 bar and (c) 40 bar ambient pressure of spray chamber.

Spray penetration is significantly influenced by fuel injection pressure and spray chamber pressure. Figure 4 shows the effect of fuel injection pressure on spray tip penetration. Spray tip penetration increased with increasing fuel injection pressure. After 0.4 ms elapsed time, spray penetration length for diesel between 1500 bar and 500 bar injection pressure increased by 15.55 mm (~ 38.90%) (Figure 4a). With increasing fuel injection pressure, slope of spray tip penetration curve increased and spray penetration length of 45 mm and 55 mm were attained at 20 and 40 bar ambient pressure respectively after 0.9 ms at 1500 bar fuel injection pressure for mineral diesel. At higher fuel injection pressure (1500 bar), biodiesel blends spray penetration curve showed slightly lower slope than baseline mineral diesel at 40 bar chamber pressure, suggesting its stronger atomization with smaller droplet diameters and, consequently the momentum. On the basis of these experimental results, it can be concluded that the influence of varying blending ratio on spray penetration was lower than that of varying fuel injection pressure on the spray penetration length. Siebers concluded from his study that ambient gas density has strong effects on the liquid length of the spray. An increase in gas density causes a reduction in the liquid length of the fuel spray. It was also concluded that sensitivity of liquid length decreased as density increased markedly [15]. Similar results for spray tip penetration with increasing spray chamber pressure and fuel injection pressure were reported by other researchers also [1,16].

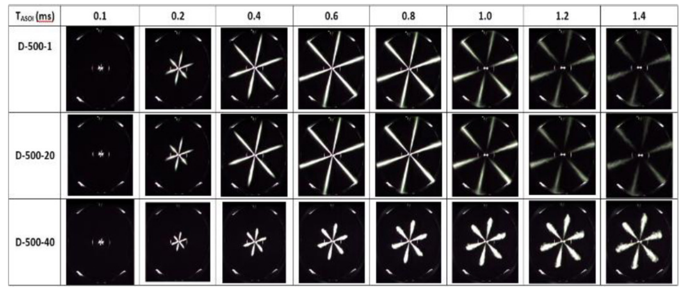


Figure 5. Effect of ambient pressure on spray evolution for diesel at 500 bar injection pressure.

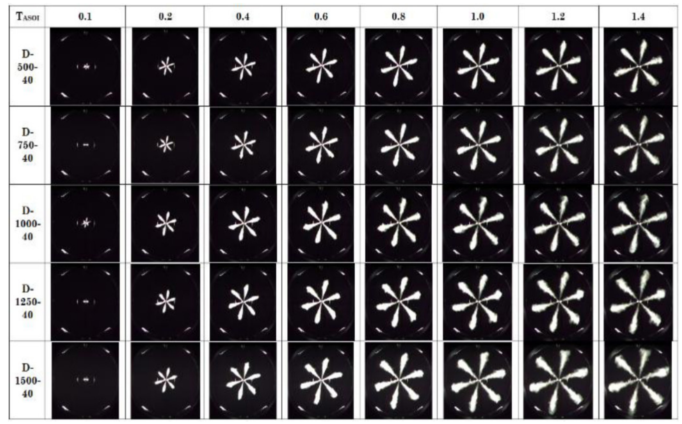


Figure 6. Effect of fuel injection pressure at 40 bar ambient pressure on diesel spray evolution.

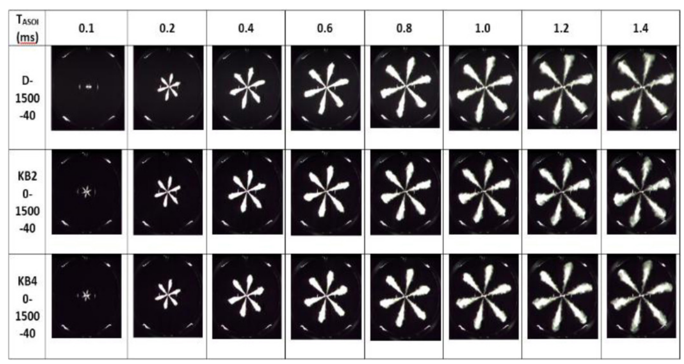


Figure 7. Comparison of spray evolution of diesel, KB20 and KB40 at 1500 bar injection pressure and 40 bar ambient pressure.

Effect of fuel injection pressure, CVSC pressure and biodiesel blending ratio on the spray evolution and development are compared in Figures 5, 6, 7 with the elapsed time after start of injection (ASOI). The spray evolution process is mainly influenced by the pressure differential between fuel injection pressure and ambient pressure in CVSC. This is illustrated by the images (Figures 5-6), spray penetration at a particular time decreased with increasing ambient pressure and increased with increasing fuel injection pressure. These results have been verified by spray penetration measurements shown in Figures 3-4. The effects of fuel injection pressure on the spray penetration length at constant SOI showed that the spray tip penetration remarkably increased within 0.6 ms after the SOI (Figure 6). In addition, at 1500 bar fuel injection pressure and 40 bar ambient pressure, biodiesel blends showed slight slower spray evolution compared to diesel (Figure 7). Similar results for spray tip penetration and spray evolution with increasing fuel injection pressure were reported by other researchers also [17].

## Spray Area

The projected spray area represents the fuel-air mixing quality [18]. Figures 8 and 9 compare results for spray area for mineral diesel, KB20 and KB40 at various fuel injection pressures and different ambient pressures. In order to compare the results of the spray envelope, the spray behavior is determined by the total area covered by the selected pixels on the spray image boundary. In the Figures 8-9, average spray area was obtained using data processing from 3 images (data set) captured at same condition during spray visualization.

Figure 8 compares the effect of ambient pressure in CVSC and fuel injection pressure on the spray area for diesel, KB20 and KB40 collectively. It was found that with increasing CVSC pressure, slope of spray area curves reduced for all test fuels at each injection pressure. As the time elapses after the SOI, the spray area of mineral diesel and Karanja biodiesel blends increased with increasing fuel injection pressure (Figure 9). It can be seen that spray area increased due to higher momentum of disintegrated spray droplets at higher fuel injection pressures, which induced the extension of spray region because of longer spray tip penetration [19]. Higher spray chamber pressure marginally decreased the spray area.

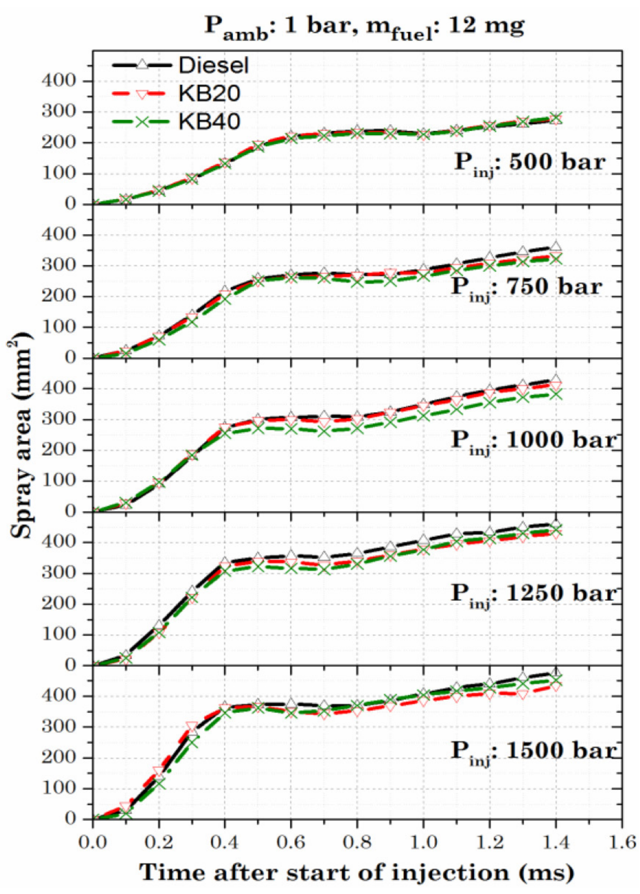


a.

Figure 8.

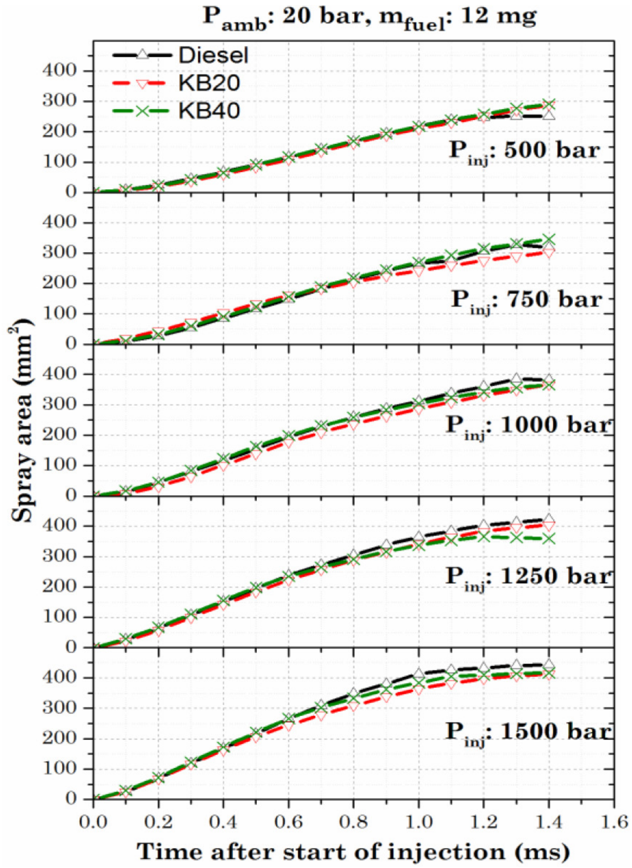


b.

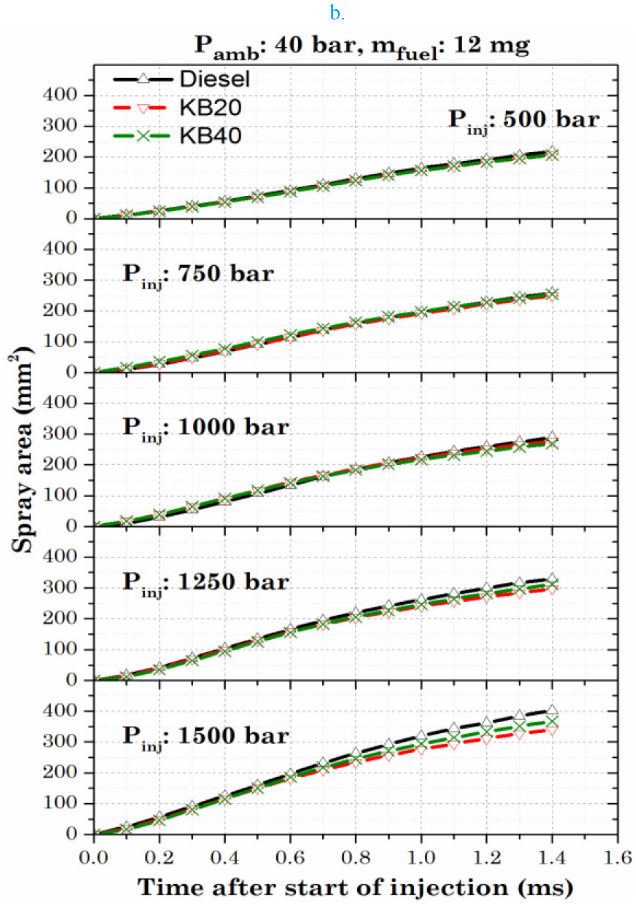


c.

Figure 8. (cont.) Effect on spray area for diesel, KB20 and KB40 blends at ambient pressure (a) 1 bar, (b) 20 bar and (c) 40 bar for different injection pressure.

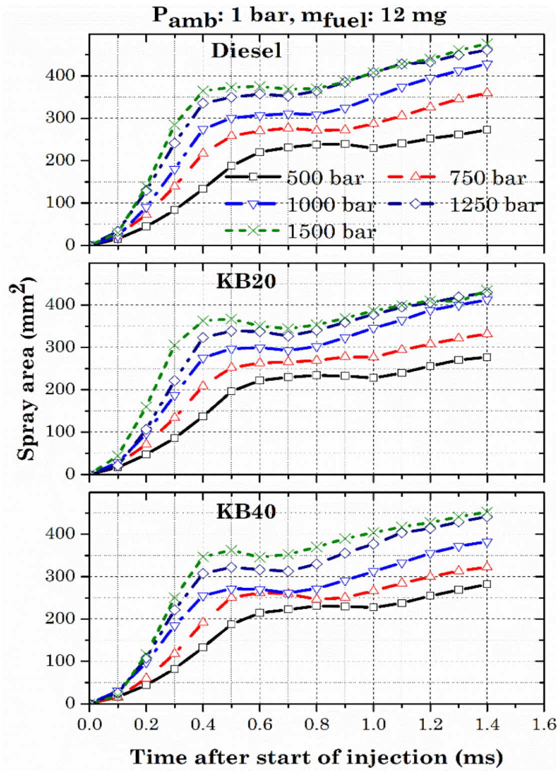


a.

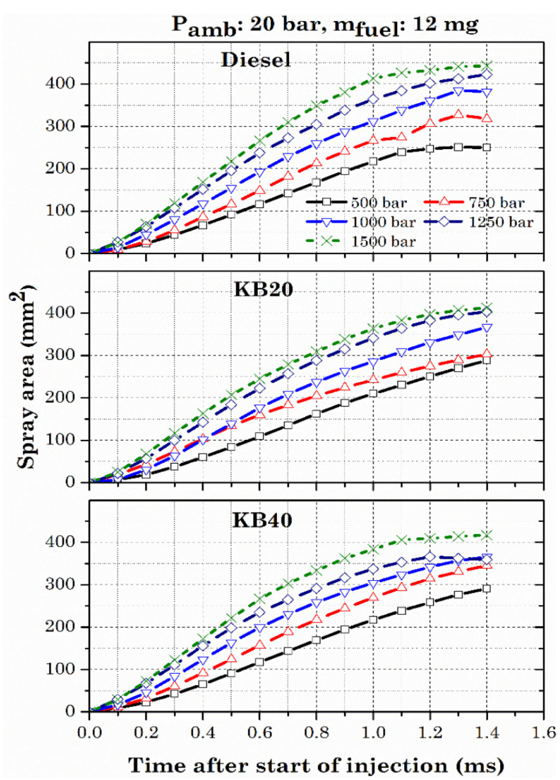


b.

Figure 9.

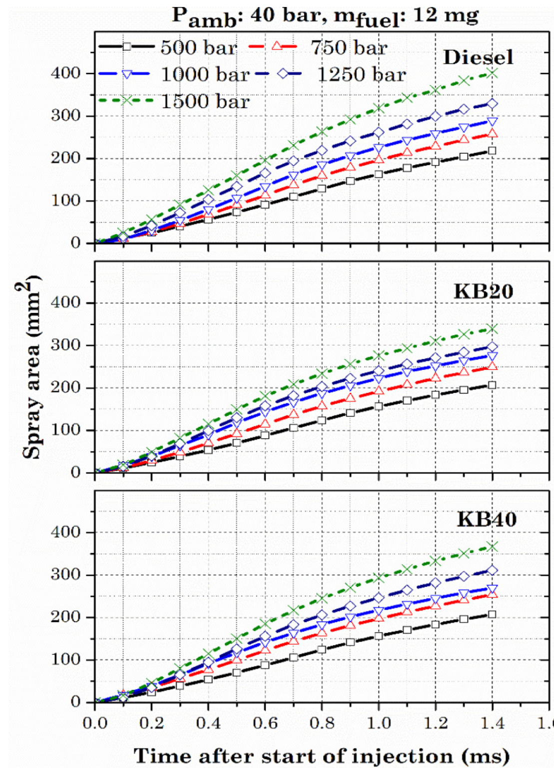


c.

Figure 9. (cont.) Effect of fuel injection pressure on spray area for diesel, KB20 and KB40 at (a) 1 bar, (b) 20 bar and (c) 40 bar chamber ambient pressure.

## Spray Cone Angle

Figures 10-11 compare spray cone angle for diesel, KB20 and KB40 under different fuel injection pressure and chamber ambient pressure.

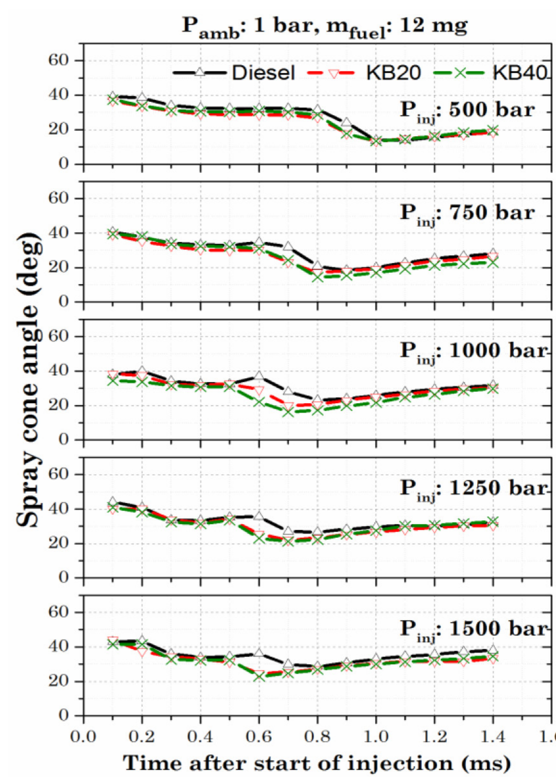


a.

Figure 10. Effect of ambient pressure on spray cone angle for diesel, KB20 and KB40 blends at (a) 1 bar, (b) 20 bar and (c) 40 bar spray chamber pressure.

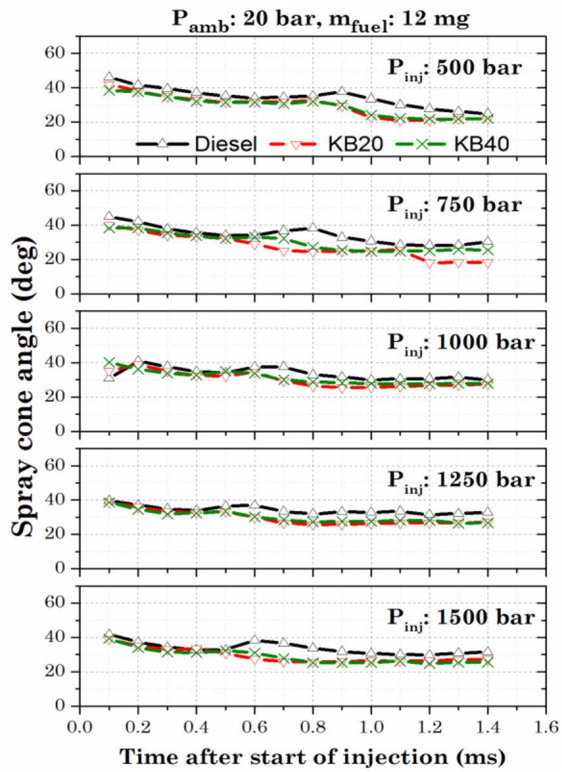


b.

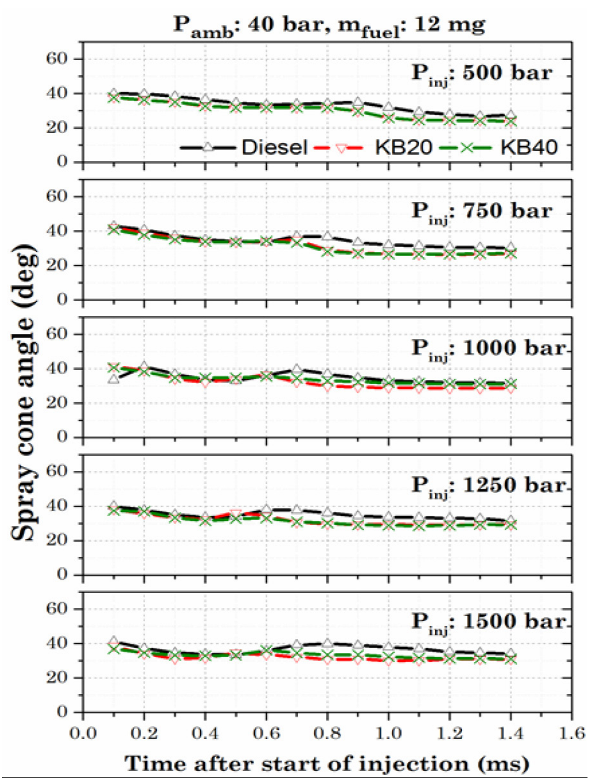


c.

Figure 10. (cont.) Effect of ambient pressure on spray cone angle for diesel, KB20 and KB40 blends at (a) 1 bar, (b) 20 bar and (c) 40 bar spray chamber pressure.

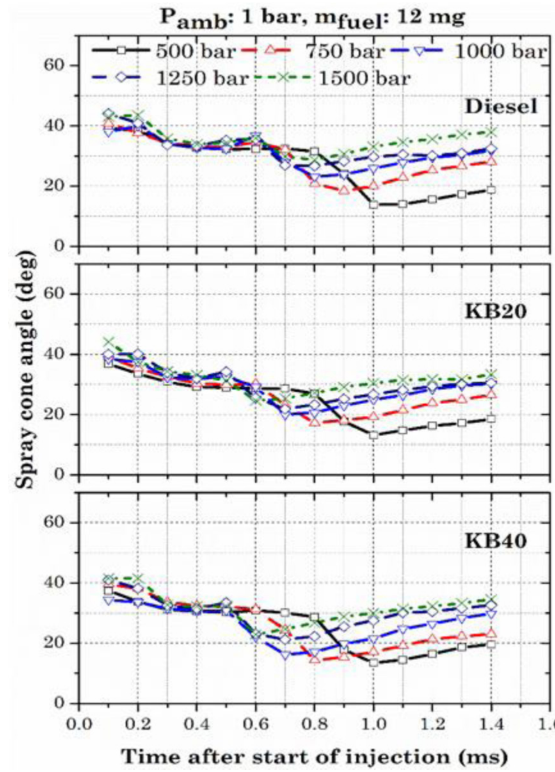


a.

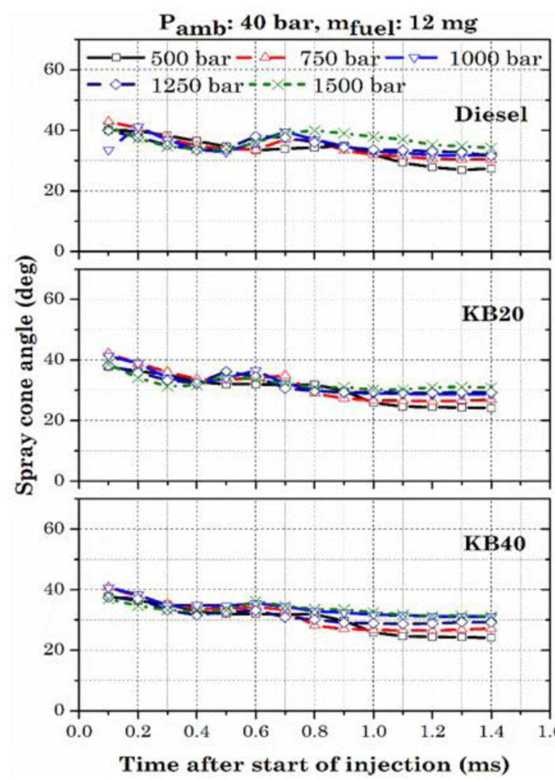


b.

Figure 11. Effect of fuel injection pressure (500, 750, 1000, 1250 and 1500 bar) on spray cone angle for diesel, KB20 and KB40 blends at (a) 1 bar, (b) 20 bar and (c) 40 bar spray chamber pressure.

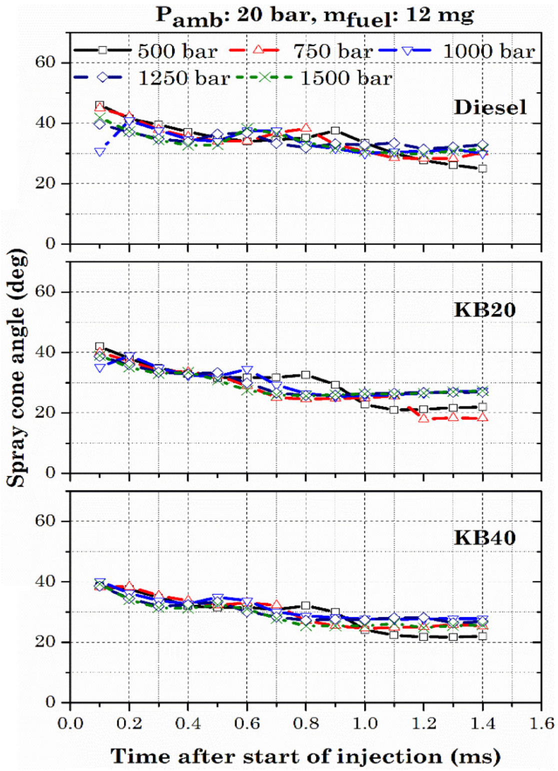


c.

Figure 11. (cont.) Effect of fuel injection pressure (500, 750, 1000, 1250 and 1500 bar) on spray cone angle for diesel, KB20 and KB40 blends at (a) 1 bar, (b) 20 bar and (c) 40 bar spray chamber pressure.

To show a reliable comparison of spray cone angles, the cone angle of each plume was averaged. Curves at different fuel injection pressures showed similar trend for all test fuels. The cone angle fluctuated at the beginning of the injection and then decreased to a relatively steady state 1.0 ms after SOI (Figure 10). This trend shows the effect of spray evolution with nearly unchanged width of the plume. Once the momentum of liquid droplets reaches a balance with ambient pressure, the cone angle attains an approximately constant value. The spray cone angle increased with increasing ambient pressure in CVSC (Figure 10). Higher ambient pressure applies more resistance on the fuel spray, and obstructs its axial development thus compelling the spray to develop transversely. The spray cone angles of diesel were slightly wider than biodiesel blends (Figure 10). However, this difference was not significant. It was also explained by Hiroyasu and Arai [20] that the spray cone angle is inversely proportional to the fuel density. The spray cone angle increased slightly with increasing fuel injection pressure (Figure 11). It was proved by several researchers that diesel spray cone angle is only marginally influenced by the fuel injection pressure and remains constant during the entire injection [18,20]. However, the chamber atmosphere pressure/ density directly affect the spray angle, which becomes wider in a dense, high pressure ambient environment [18]. At the closing of injection, spray cone angel decreased however it was relatively higher at higher fuel injection pressure (Figure 11a) and ambient pressure (Figure 11b-c).

Generally, higher fuel injection pressure results in increased spray tip penetration, spray area and spray cone angle, while the rise of ambient pressure results in the decreased spray tip penetration, spray area and increased spray cone angle [14]. Conclusively from the macroscopic spray view point, shape of biodiesel blends spray is not significantly different from that of mineral diesel.

### *Microscopic Spray Characteristics*

Microscopic spray characteristics of biodiesel blend (KB20 and KB40) such as spray droplet diameter and axial velocity distributions were compared with that of baseline mineral diesel using Phase Doppler Interferometry (PDI). The investigations of test fuels were conducted 40 mm down-stream from the nozzle at different injection pressures and ambient pressure in CVSC. Lee and Park [2] reported from their experimental and numerical study that beyond 40 mm downstream from the nozzle tip, SMD and axial mean velocity were found in regular distribution, because the rates of disintegration and coalescence were similar at 800 bar fuel injection pressure. Fuel's atomization characteristics in an engine's combustion chamber directly affect the combustion and emission characteristics of the engine.

### *Spray Droplet Velocity Distribution (3D)*

Figures 12a-c represents the scatter plot of fuel spray droplet diameter and axial velocity at 40 mm downstream of the spray injector nozzle. These figures indicate the diameter to velocity correlation (DVC) of the fuel droplets injected. Since the PDI instrument responds to droplet flux, the relative velocity of the droplets also affects droplet size distribution. To convert the size distribution to a concentration dependent distribution, the numbers of counts in each size were normalized to remove the effect of the droplet velocity for each size class by the system software (AIMS). Each point on the graph is a single drop measurement for droplet size and velocity. As spray comes out of the injector nozzle, the droplets outside the main spray plume disintegrate into the smaller droplet before the inner droplets because of the large relative velocity between the spray and ambient air [2]. Small size and high velocity of spray droplets produced by the primary and secondary breakup of the spray plume [21]. The small size of the droplets can be attributed to secondary atomization [21].

In Figure 12, size distribution indicate that Karanja biodiesel blends produced a higher number of larger droplets than mineral diesel, which is due to difference in the physical properties of the test fuels [21]. The droplet peak velocity increased as the fuel injection pressure increased. However, peak velocity was observed to be lower at 1500 bar, which may be due to incomplete atomization of fuel 40 mm downstream of the nozzle at higher injection pressures. Peak velocity distribution was higher for smaller droplets of mineral diesel compared to biodiesel blends. However, higher number of larger size droplets of biodiesel blends showed higher velocity due to their greater momentum.

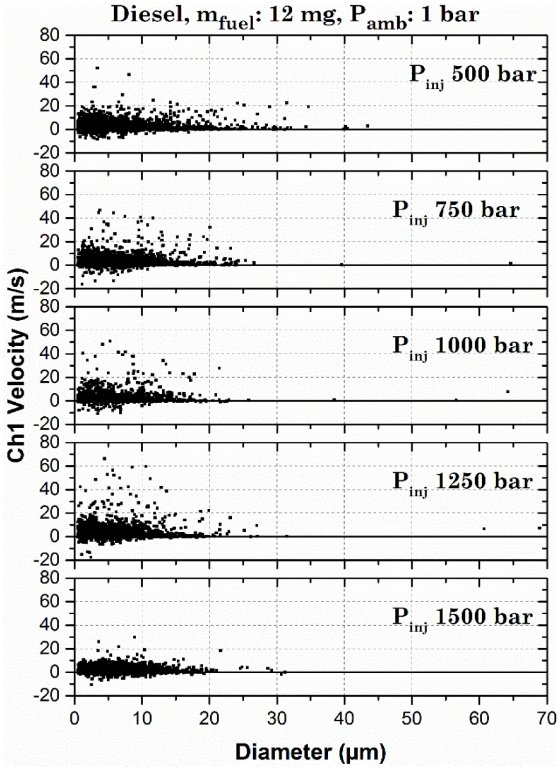


a.

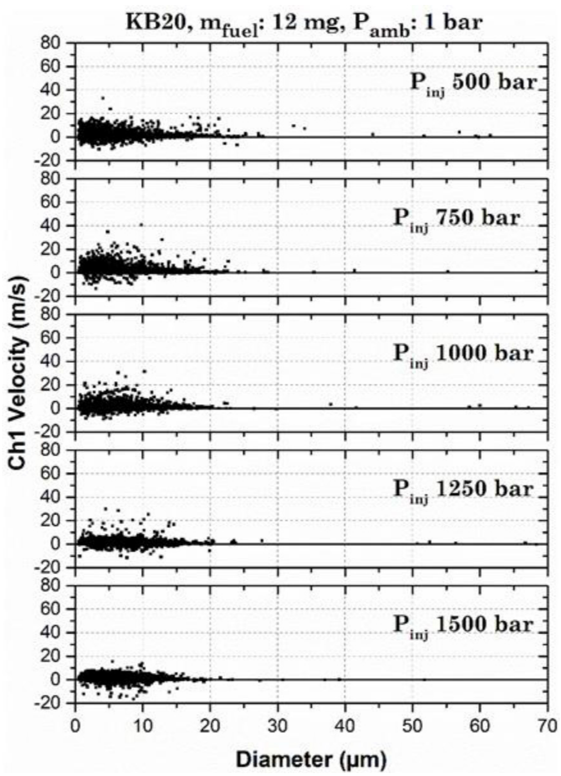


b.

Figure 12.

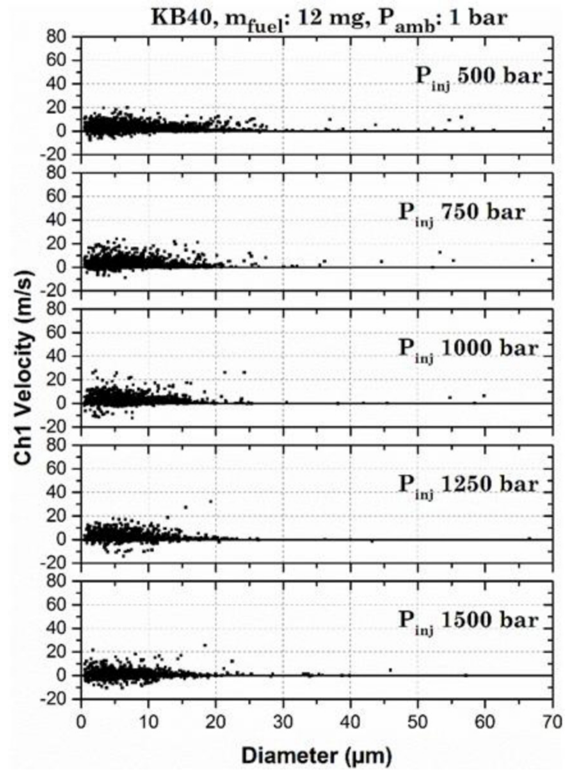


c.

Figure 12. (cont.) Scatter plot of droplet diameter and axial velocity for (a) Diesel, (b)

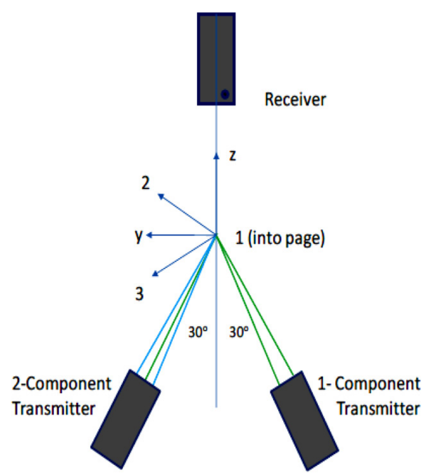


Figure 13. Configuration of spray in X-, Y- and Z- directions.

Velocity components of spray droplets from the nozzle in X-, Y- and Z- directions are shown in Figure 13. In three dimensional (3D) PDI, it is seldom possible to configure the optics to measure three orthogonal velocity components. The software (AIMS) used in PDI system transforms the measured non-orthogonal velocities into orthogonal components, which represents the velocity in orthogoanl coordinate system from channel 1, 2 and 3 measurements [12]. Figures 14, 15, 16 show the spray droplet velocity distribution histogrms measured by Channel 1, 2 and 3 (X-, Y- and Z- components of velocity) for KB20, KB40 and mineral diesel.

In Figures 14, 15, 16, maximum number of count were observed for zero velocity in all three channels. In between two injections, droplets remain suspended in the probe volume and are detected by the PDI receiver. Although the velocities observed increased with increasing fuel injection pressures, maximum droplet velocity was found in channel 1, which was upto 50 m/s as shown in Figure 12. Droplets velocities from mineral diesel were relatively higher than biodiesl blends. Channel 3 showed droplet velocity component in -Z direction, since the spray was inclined vertically in downward direction.

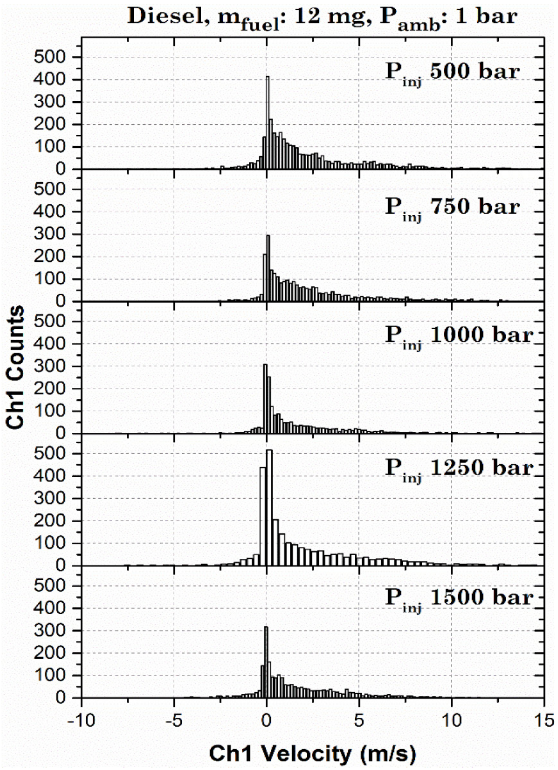


a.

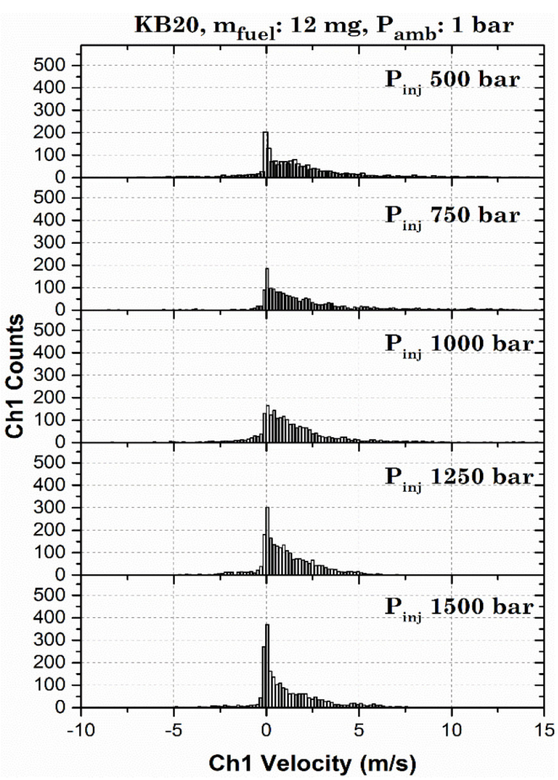


b.

Figure 14.

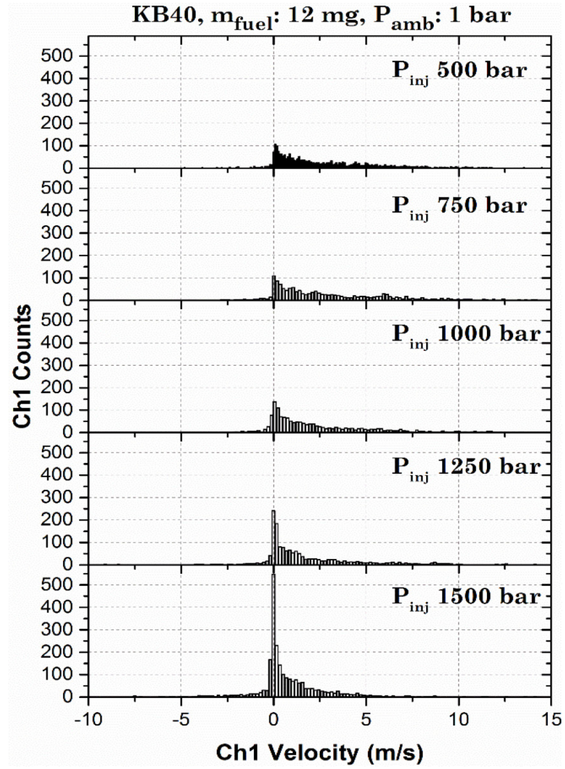


c.

Figure 14. (cont.) Channel 1 droplet velocities histogram 40mm downstream from the nozzle at different injection pressures for (a) Diesel, (b) KB20, and (c) KB40.

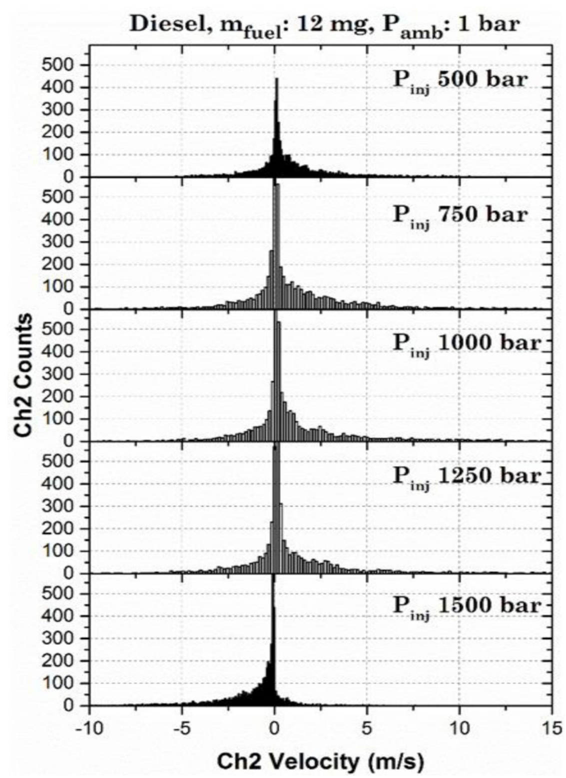


a.

Figure 15. Channel 2 droplet velocities histogram 40mm downstream from the nozzle at different injection pressures for (a) Diesel, (b) KB20, and (c) KB40.

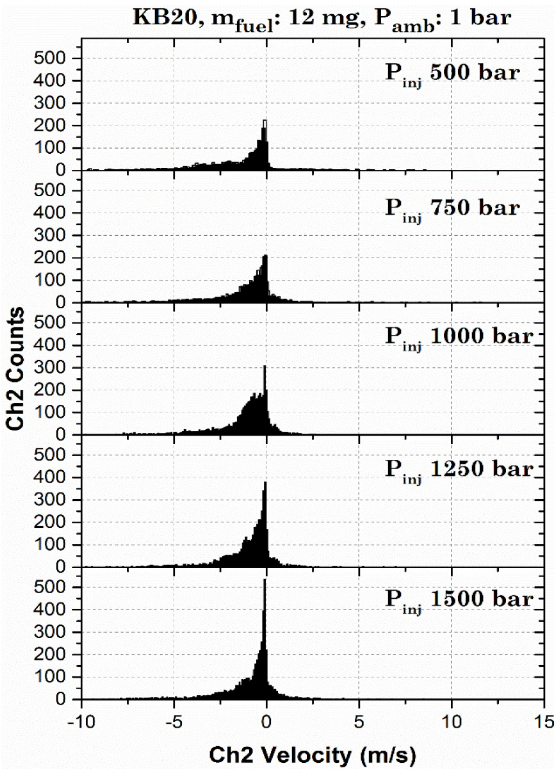


b.

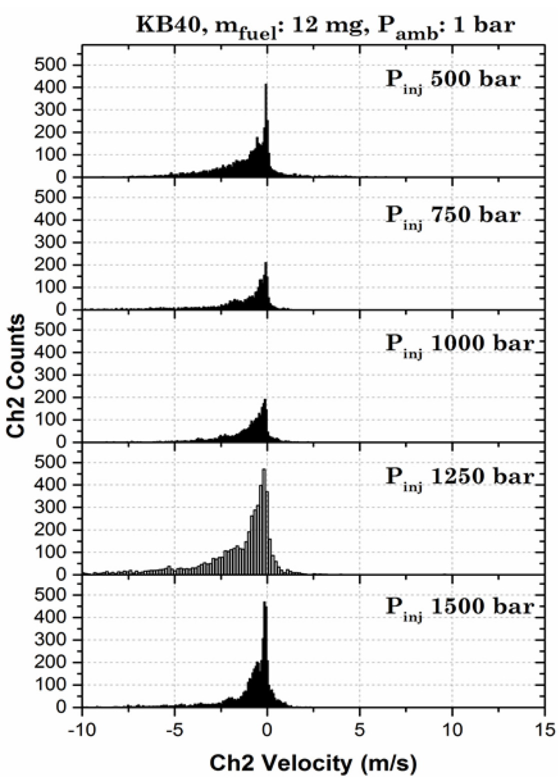


c.

Figure 15. (cont.) Channel 2 droplet velocities histogram 40mm downstream from the nozzle at different injection pressures for (a) Diesel, (b) KB20, and (c) KB40.

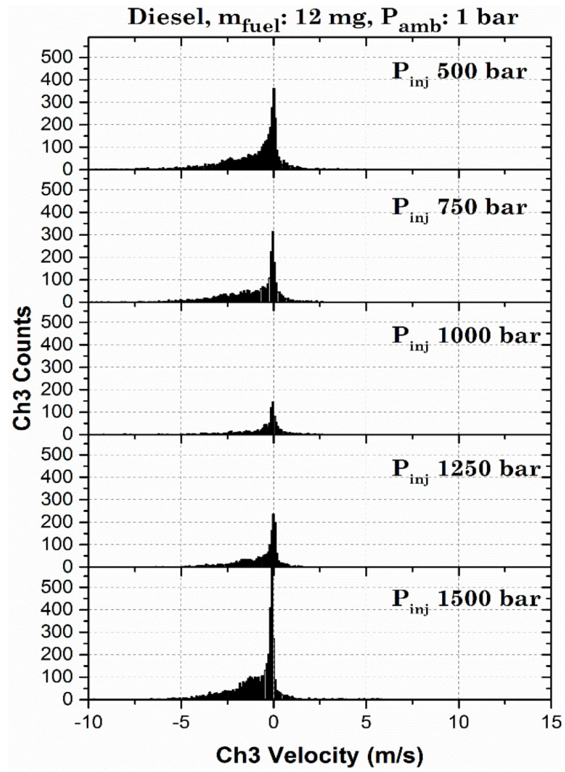


a.

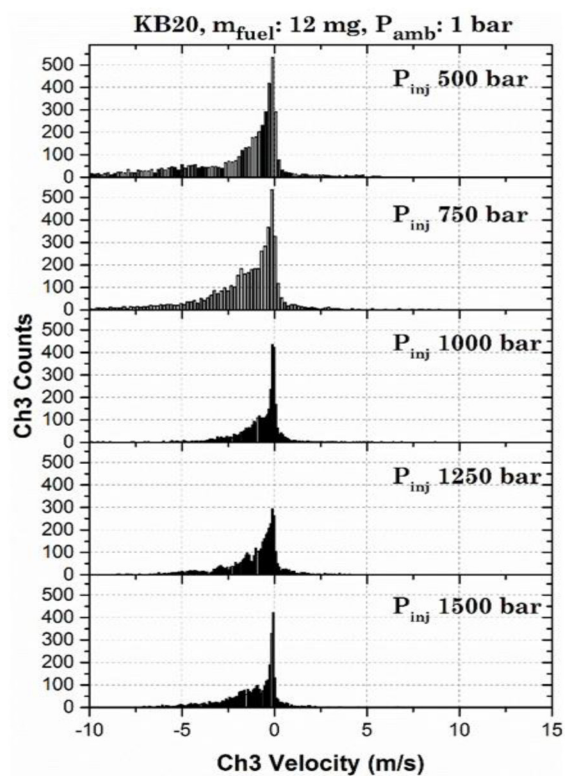


b.

Figure 16. Channel 3 droplet velocities histogram 40mm downstream from the nozzle at different injection pressures for (a) Diesel, (b) KB20, and (c) KB40.

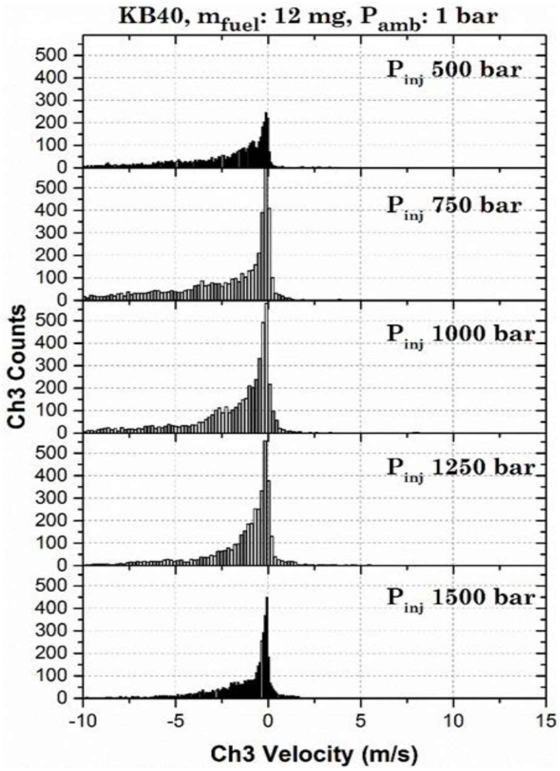


c.

Figure 16. (cont.) Channel 3 droplet velocities histogram 40mm downstream from the nozzle at different injection pressures for (a) Diesel, (b) KB20, and (c) KB40.

## Spray Droplet Size Distribution

Due to different surface tension and viscosity of biodiesel compared to mineral diesel, it is beneficial to analyze Sauter mean diameter (SMD or $D_{32}$) and arithmetic mean diameter (AMD or $D_{10}$) for biodiesel spray droplets. Figure 17 shows the droplet diameters (SMD and AMD) in the fuel spray of Karanja biodiesel blends and conventional diesel, measured by the PDI system. As shown in Figure 17, droplet sizes represented by SMD or $D_{32}$ and AMD or $D_{10}$ increased with increasing biodiesel concentration in the test fuel. Suh *et al.* also reported higher Sauter mean diameter for biodiesel than conventional diesel because of its high viscosity and surface tension [16]. Higher surface tension of biodiesel causes lower Weber number of biodiesel, which is the main reason for higher SMD distributions [8]. Higher kinematic viscosity of biodiesel increases the friction between the nozzle surface and the fuel and reduces the fuel injection velocity of the biodiesel blends. This lower injection velocity of biodiesel is one of the reasons for increased SMD for biodiesel blended fuels [8].

Droplet size distribution decreased with increasing fuel injection pressure for Karanja biodiesel blends vis-à-vis baseline mineral diesel. The trend observed is consistent with other studies reported in the literatures [3,22]. It was also observed that the mean diameter of higher Karanja biodiesel blends were significantly different compared to mineral diesel. KB40 demonstrated significantly larger droplet sizes than mineral diesel as shown in Figure 17. At 1500 bar fuel injection pressure, AMD for test fuels was observed higher than relatively lower fuel injection pressure (Figure 17b), which may be due to presence of fuel ligaments at the measurement point 40 mm downstream of the nozzle, leading to inadequate atomization, consequently resulting in higher AMD.

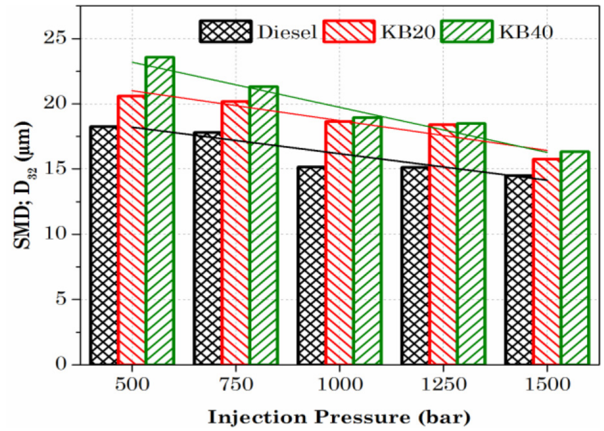


a. Sauter mean diameter

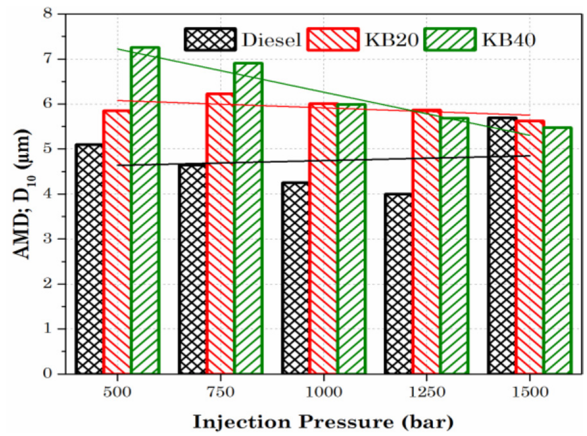


b. Arithmetic mean diameter

Figure 17. (a) Sauter mean diameter and (b) Arithmetic mean diameter of Karanja biodiesel blends vis-à-vis mineral diesel.

Figure 18 shows the histograms for droplet diameter distributions for the measured fuel sprays. The largest droplets in the spray were ~ 30 μm in diameter for the test fuels. However maximum number counts were observed for < 10 μm diameter droplets. Higher number counts for smaller droplets were observed for diesel spray, while higher diameter range was found for biodiesel blends. This behavior can also be verified by looking at the droplet size-velocity correlation shown in Figure 12. Figures 19 are similar to Figures 18, except that the data has been corrected for the effect of varying sample volume on the drop size. Figure 19 show histograms for probe volume corrected number density vs. size distribution. The probe volume corrected count is a correction applied to account for dependence of the probe volume on the droplet size [23]. Since smaller droplets have a smaller effective sample volume, the number in each size bin must be increased by a factor equal to the ratio of the sample volume for the largest drops to the sample volume for the drops in each size bin. This normalization approach compensates for the sample volume effect by increasing the number of droplets in the smaller size bins.

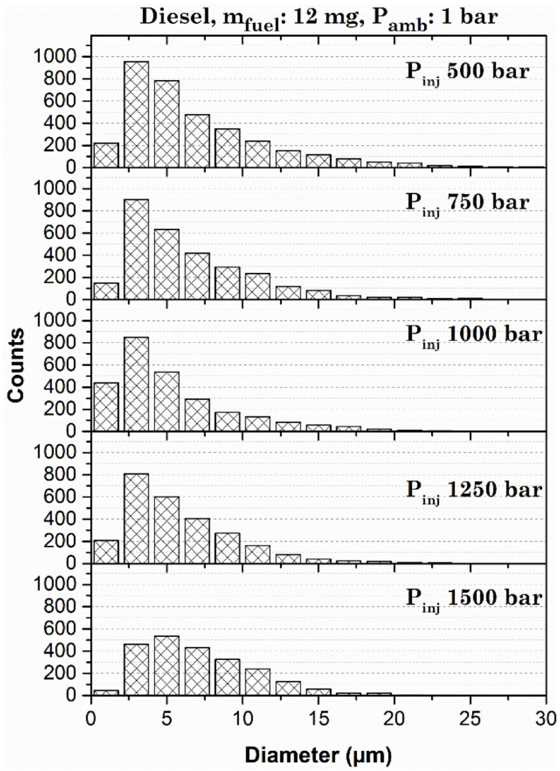


a.

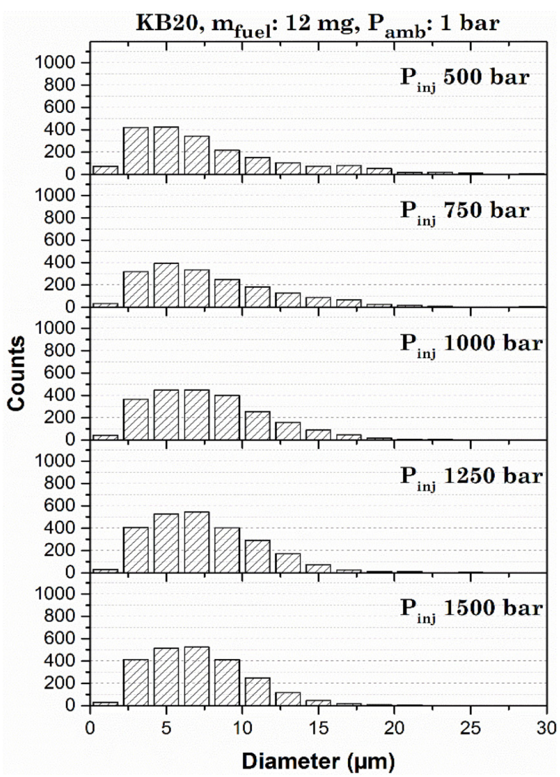


b.

Figure 18.

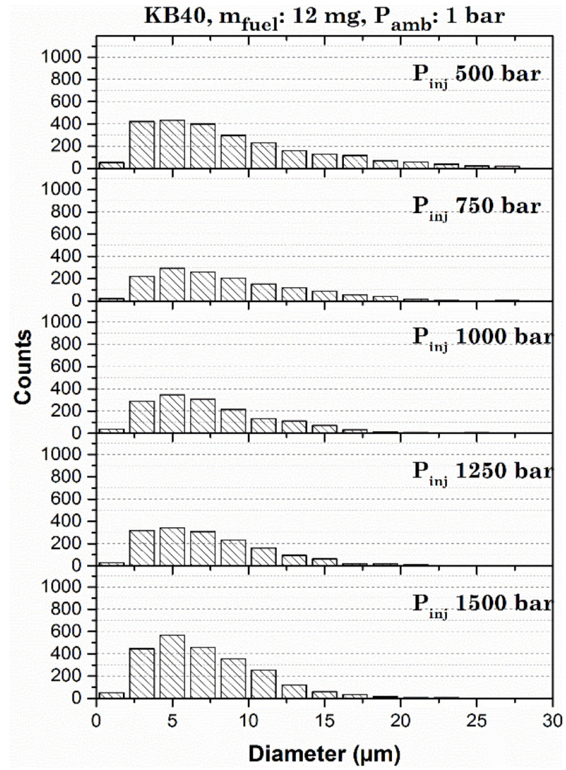


c.

Figure 18. (cont.) Droplet size distribution histogram of (a) Diesel, (b) KB20 and (c) KB40 sprays.

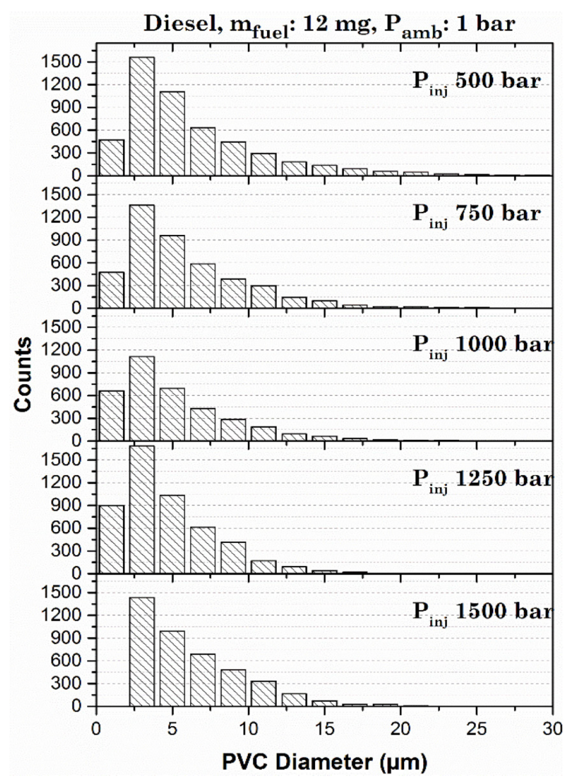


a.

Figure 19. Droplet size distribution histogram of the fuel injection with probe volume correction (PVC) from (a) Diesel, (b) KB20 and (c) KB40.

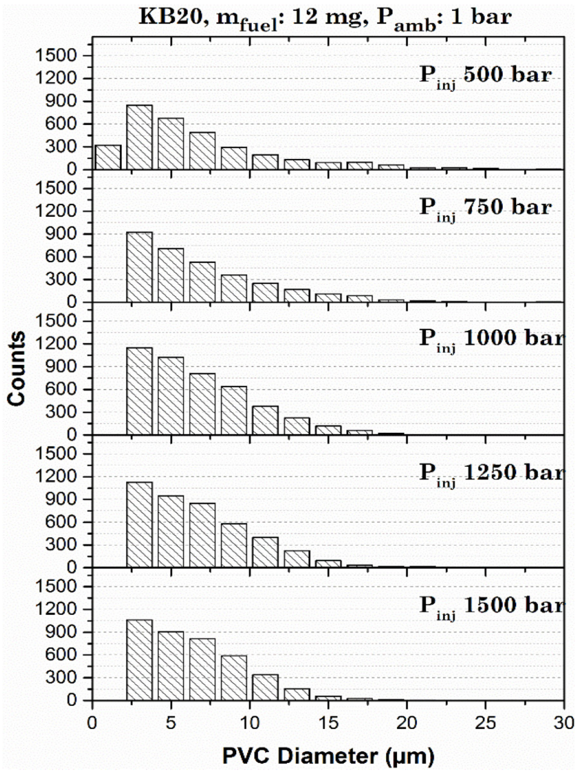


b.

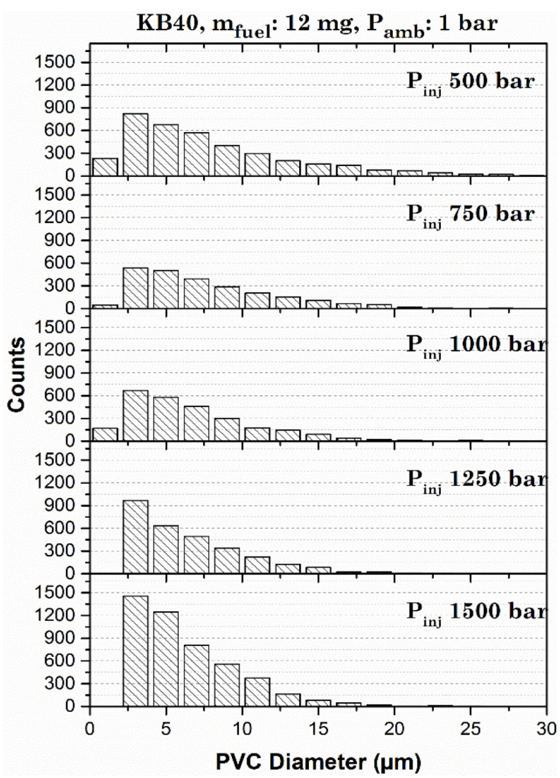


c.

Figure 19. (cont.) Droplet size distribution histogram of the fuel injection with probe volume correction (PVC) from (a) Diesel, (b) KB20 and (c) KB40.

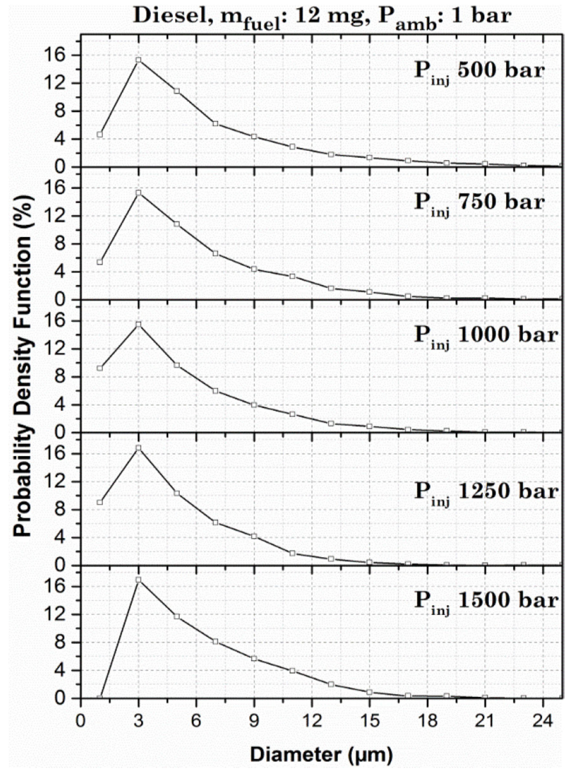


a.

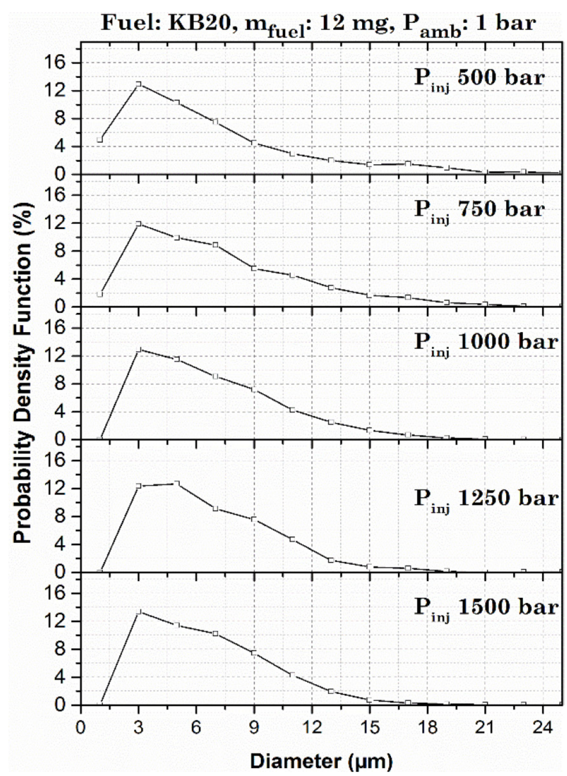


b.

Figure 20. Probability density function of droplet diameters from (a) Diesel, (b) KB20 and (c) KB40.

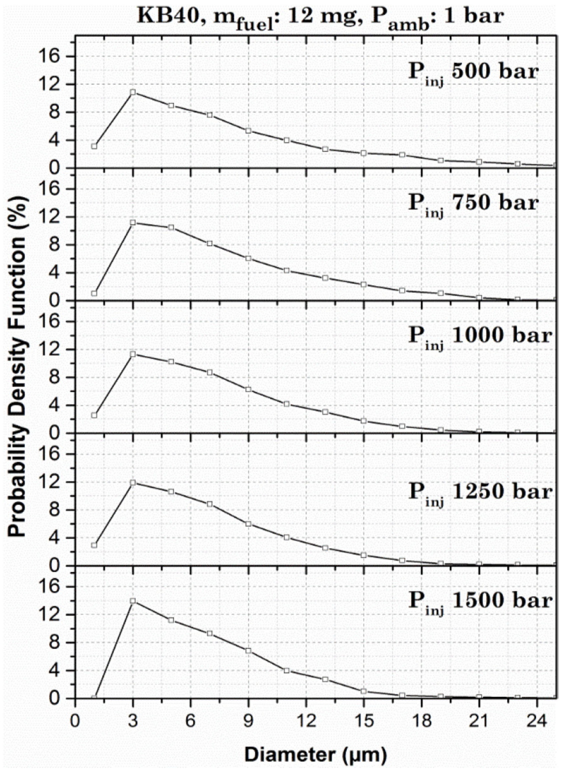


c.

Figure 20. (cont.) Probability density function of droplet diameters from (a) Diesel, (b) KB20 and (c) KB40.

The sample volume correction is important for an exact measurement of the droplet size distribution. Figures 18 and 19, show similar trends for diameter distribution with change of fuel injection pressures and test fuels. At similar injection pressure, number counts were lower with increasing ratio of biodiesel blends. Figure 20 shows the droplet size probability density function (PDF) distribution at varying injection pressure for KB20 and KB40 vis-à-vis baseline diesel. The PDFs were evaluated based on single droplet characteristics measured by PDI method over multiple injection cycles [24]. It was observed that increasing fuel injection pressures clearly impacts droplet size PDF distribution, which increased with increasing fuel injection pressure for all test fuels. The droplet size distribution peak was seen to be at 2-3 µm for all test fuels. Similar trends for solenoid injectors with increasing fuel injection pressures were reported by Nithyanandan *et al.* [25]. The differences between the distributions were more pronounced with biodiesel blends, for which, distribution were more skewed to the right than mineral diesel. This is consistent with the expectation that the atomization of biodiesel blends is inhibited by its higher viscosity and surface tension [21].

## Conclusions

In the present study, spray evolution using macroscopic and microscopic techniques was done at varying fuel injection pressure and ambient pressure in a constant volume spray chamber using CRDI engine injector (Delphi; Solenoid CRDI injector) for Karanja biodiesel blends (KB20 and KB40) and mineral diesel. Density of Karanja biodiesel was relatively higher than mineral diesel and it was within the specified ASTM limits. Viscosity of Karanja biodiesel at 40°C was relatively higher than mineral diesel. Calorific value of Karanja biodiesel was ~14% lower than baseline mineral diesel. Viscosity and density of the test fuels (KB20 and KB40) were higher than mineral diesel, while calorific value was relatively lower. Higher fuel injection pressure increased the spray tip penetration, spray area and spray cone angle while the higher ambient pressure in the constant volume spray chamber shortened the spray tip penetration, spray area and increased the spray cone angle.

Karanja biodiesel blends produced higher number of larger droplets than mineral diesel. Droplet peak velocity was found to be increased with increasing fuel injection pressure; however it was lower at 1500 bar possibly due to incomplete atomization of fuel at 40 mm downstream of the nozzle. Sauter mean diameter (SMD or $D_{32}$) and arithmetic mean diameter (AMD or $D_{10}$) was decreased with increasing injection pressure, however increased with increasing biodiesel concentration in the test fuel. Higher droplet size for biodiesel blends was observed probably due to higher viscosity and surface tension. As per sample or probe volume correction lower number count was found with increasing ratio of biodiesel blends.

Conclusively from macroscopic parameter view point, shape of biodiesel blend spray was not significantly different from the baseline diesel spray. This study suggests that biodiesel blends are comparable to mineral diesel, as far as microscopic and macroscopic spray characterization is concerned.

## References


1. Senatore, A., Cardone, M., Allocca, L., Vitolo, S. et al., "Experimental Characterization of a Common Rail Engine Fuelled with Different Biodiesel," SAE Technical Paper 2005-01-2207, 2005, doi:10.4271/2005-01-2207.
2. Lee, C. S., and Park, S. W., “An experimental and numerical study on fuel atomization characteristics of high-pressure diesel injection sprays,” Fuel, 81: 2417-2423, 2002.
3. Lacoste, J., Crua, C., Heikal, M., Kennaird, D. et al., "PDA Characterisation of Dense Diesel Sprays Using a Common-Rail Injection System," SAE Technical Paper 2003-01-3085, 2003, doi:10.4271/2003-01-3085.
4. Wang, X., Huang, Z., Kuti, O. A., Zhang, W., and Nishida, K., “Experimental and analytical study on biodiesel and diesel spray characteristics under ultra-high injection pressure,” Int. J. Heat Fluid Flow, 31: 659-666, 2010.
5. Park, S. H., Cha, J., Kim, H. J., and Lee, C. S., “Effect of early injection strategy on spray atomization and emission reduction characteristics in bioethanol blended diesel fuelled engine,” Energy, 39: 375-387, 2012.
6. Kegl, B., “Influence of biodiesel on engine combustion and emission characteristics,” Applied Energy, 88: 1803-1812, 2011.
7. Som, S., Longman, D. E., Ramírez, A. I., and Aggarwal, S. K., “A comparison of injector flow and spray characteristics of biodiesel with petrodiesel,” Fuel, 89: 4014-4024, 2010.

8. Lee, C. S., Park, S. W., and Kwon, S. I., "An Experimental Study on the Atomization and Combustion Characteristics of Biodiesel-Blended Fuels," Energy and Fuels, 19: 2201-2208, 2005.
9. Li, Y., Tian, G., Zhang, J., and Xu, H., "Comparative Experimental Study on Microscopic Spray Characteristics of RME, GTL and Diesel," SAE Technical Paper 2010-01-2284, 2010, doi:10.4271/2010-01-2284.
10. Bachalo, W., "A Method for Measuring the Size and Velocity of Spheres by Dual Beam Light Scatter Interferometry," Applied Optics, 19(3), 1980.
11. Bachalo, W., and Houser, M., "Phase Doppler Spray Analyzer for Simultaneous Measurements of Drop Size and Velocity Distributions," Optical Engineering, 23(5), 1984.
12. Operation of the Phase Doppler Interferometer (PDI) For Spray Drop Size and Velocity measurement, PDI-300 MD User Manual, Artium Technologies, Inc., USA.
13. Zhu, J., Kuti, O., and Nishida, K., "Effects of Injection Pressure and Ambient Gas Density on Fuel - Ambient Gas Mixing and Combustion Characteristics of D.I. Diesel Spray," SAE Technical Paper 2011-01-1819, 2011, doi:10.4271/2011-01-1819.
14. He, C., Ge, Y., Tan, J., and Han, X., "Spray properties of alternative fuels: A comparative analysis of biodiesel and diesel," International journal of energy research, 32(14), 1329-1338, 2008.
15. Siebers, D., "Liquid-Phase Fuel Penetration in Diesel Sprays," SAE Technical Paper 980809, 1998, doi:10.4271/980809.
16. Suh, H.K., Roh, H. G., and Lee, C. S., "Spray and combustion characteristics of biodiesel/ diesel blended fuel in a direct injection common-rail diesel engine," J Eng Gas Turbines Power, 130(3):1-9, 2008.
17. Uhl, M., Schießl, R., Maas, U., and Dreizler, A., "Time Resolved Spray Characterisation in a Common Rail Direct-Injection Production Type Diesel Engine Using Combined Mie/LIF Laser Diagnostics," SAE Technical Paper 2003-01-1040, 2003, doi:10.4271/2003-01-1040.
18. Delacourt, E., Desmet, B., and Besson, B., "Characterisation of very high pressure diesel sprays using digital imaging techniques," Fuel, 84(7): 859-867, 2005.
19. Agarwal, A. K., Dhar, A., Gupta, J. G., Kim, W. I., Lee, C. S., and Park, S. W., "Effect of fuel injection pressure and injection timing on spray characteristics and particulate size-number distribution in a biodiesel fuelled common rail direct injection diesel engine," Applied Energy, 130: 212-221, 2014.
20. Hiroyasu, H. and Arai, M., "Structures of Fuel Sprays in Diesel Engines," SAE Technical Paper 900475, 1990, doi:10.4271/900475.
21. Crua, C., De-Sercey, G., Heikal, M., and Gold, M., "Drop sizing of near-nozzle diesel and RME sprays by microscopic imaging," ICLASS 2012, 12th Triennial International Conference on Liquid Atomization and Spray Systems, Heidelberg, Germany, 2012.
22. Koo, J. and Martin, J., "Droplet Sizes and Velocities in a Transient Diesel Fuel Spray," SAE Technical Paper 900397, 1990, doi:10.4271/900397.
23. Widmann, J. F., Presser, C., and Leigh, S. D., "Improving phase Doppler volume flux measurements in low data rate applications," Meas. Sci. Technol., 12:1180-1190, 2001.
24. Fukumasu, N. K., Yanagihara, J. I., and Krieger Filho G. C., "Influence of fuel injection frequency on droplet dispersion in ethanol pulsed spray flames," Applied Thermal Engineering, 81:198-209, 2015.
25. Nithyanandan, K., Hou, D., Major, G., and Lee, C., "Spray Visualization and Characterization of a Dual-Fuel Injector using Diesel and Gasoline," *SAE Int. J. Fuels Lubr.* 7(1):144-158, 2014, doi:10.4271/2014-01-1403.


## Contact Information


Prof. Avinash Kumar Agarwal, FSAE, FASME
Poonam and Prabhu Goyal Endowed Chair Professor
Department of Mechanical Engineering
Indian Institute of Technology Kanpur
Kanpur-208016 India
Home Page: www.iitk.ac.in/erl
akag@iitk.ac.in
Tel: +91 512 2597982 (Off)
+91 512 2598682 (Res)
Fax: +91 512 2597982, 2597408 (Off)

Jai Gopal Gupta
Research Scholar, Department of Mechanical Engineering
Indian Institute of Technology Kanpur
Kanpur-208016 India
Current affiliation:
Govt. Women Engineering College, Ajmer- 305002 India
jaig@iitk.ac.in
jaigopalg@gmail.com
Tel: +91 145-2695535


## Acknowledgments


The Grants from Department of Science and Technology (INT/ROK/IKRI-9 /2013), Government of India, and National Research Foundation of Korea (NRF), Ministry of Education, Science and Technology (MEST), the Republic of Korea, for internship are highly acknowledged. We are also thankful to Combustion Engine and Energy Conversion Laboratory, Hanyang University, Seoul, South Korea for carrying out some experiments of this study.


## Definitions/Abbreviations

**3D** - Three dimensional

**AIMS** - Automated instrument management system

**AMD** - Arithmetic mean diameter

**ASOI** - After start of injection

**CRDI** - common rail direct injection

**CVSC** - Constant volume spray chamber

**DICI** - Direct injection compression ignition

**DPSS** - Diode-pumped solid-state

**DVC** - Diameter to velocity correlation

**FIP** - Fuel injection pressure

**GTL** - Gas-to-Liquid

**LHV** - Lower heating value

**PDF** - Probability density function

**PDI** - Phase Doppler interferometry

**PVC** - Probe volume correction

**RME** - Rapeseed methyl ester

**SMD** - Sauter mean diameter

**UFO** - Used fried oils

The Engineering Meetings Board has approved this paper for publication. It has successfully completed SAE's peer review process under the supervision of the session organizer. The process requires a minimum of three (3) reviews by industry experts.



ISSN 0148-7191

http://papers.sae.org/2016-01-0869